



MEMORANDUM FOR PR (Contractor/In-House Publication)

FROM: PROI (TI) (STINFO)

22 May 2000

SUBJECT: Authorization for Release of Technical Information, Control Number: **AFRL-PR-ED-TP-2000-118**  
B. Chehroudi (ERC); D. Talley, R. Cohn, "Experiences on Cryogenic Injection under Supercritical Condition"

**8<sup>th</sup> International Conference on Liquid Atomization and Spray Systems** (Statement A)  
**(Pasadena, CA, 17-20 Jul 00)** (Submission Deadline: 31 May 00)

1. This request has been reviewed by the Foreign Disclosure Office for: a.) appropriateness of distribution statement, b.) military/national critical technology, c.) export controls or distribution restrictions, d.) appropriateness for release to a foreign nation, and e.) technical sensitivity and/or economic sensitivity.

Comments: \_\_\_\_\_  
\_\_\_\_\_  
\_\_\_\_\_

Signature \_\_\_\_\_ Date \_\_\_\_\_

2. This request has been reviewed by the Public Affairs Office for: a.) appropriateness for public release and/or b) possible higher headquarters review.

Comments: \_\_\_\_\_  
\_\_\_\_\_  
\_\_\_\_\_

Signature \_\_\_\_\_ Date \_\_\_\_\_

3. This request has been reviewed by the STINFO for: a.) changes if approved as amended, b.) appropriateness of distribution statement, c.) military/national critical technology, d.) economic sensitivity, e.) parallel review completed if required, and f.) format and completion of meeting clearance form if required

Comments: \_\_\_\_\_  
\_\_\_\_\_  
\_\_\_\_\_

Signature \_\_\_\_\_ Date \_\_\_\_\_

4. This request has been reviewed by PR for: a.) technical accuracy, b.) appropriateness for audience, c.) appropriateness of distribution statement, d.) technical sensitivity and economic sensitivity, e.) military/national critical technology, and f.) data rights and patentability

Comments: \_\_\_\_\_  
\_\_\_\_\_

APPROVED/APPROVED AS AMENDED/DISAPPROVED

\_\_\_\_\_  
ROBERT C. CORLEY (Date)  
Senior Scientist (Propulsion)  
Propulsion Directorate

### Experiences on Cryogenic Injection under Supercritical Condition

B. Chehroudi\*  
ERC Inc.  
10 E. Saturn Boulevard  
Edwards AFB, CA 93524-7680

D. Talley and R. Cohn  
Air Force Research Laboratory, AFRL/PRSA  
10 E. Saturn Boulevard  
Edwards AFB, CA 93524-7680

#### ABSTRACT

Experiences learned at the AFRL on injection of cryogenic jets into sub- and supercritical conditions using shadowgraphy and Raman scattering measurements are presented here. Metamorphic behavior of the jet boundary undergoing disruption has been shown to occur near the critical point of the injected fluid. At subcritical pressures, the formation of droplets and ligaments are seen, resembling a second wind-induced liquid-jet breakup. The jet is incapable of reaching the classical full atomization regime due to existence of the critical point of the jet fluid within the operating range. At this point, the jet anatomy changes abruptly to imitate turbulent gas jet injection. The jet initial growth rate is plotted against the chamber-to-injectant density ratio, along with available data on other liquid/gaseous jets and mixing layers, producing a unique and informative graph. For supercritical conditions, our measured growth rate agrees well with a theoretical equation proposed by Dimotakis [1] and closely follows the trend of Papamoschou and Roshko [2] for incompressible but variable-density gaseous turbulent mixing layers. Fractal analysis of the jet boundary also shows a similarity to gas jet behavior with comparable fractal dimension. This is the first time quantitative evidence has been provided to support qualitative visualizations suggesting that supercritical jets appear to behave like conventional gas jets. Based on a physical hypothesis implying that at the point where gas-like behavior appears, the value of the jet interface bulge separation/formation characteristic time should be near that of gasification time, an "intuitive/smart" equation is proposed for the growth rate that agrees well with the presented experimental data for a wide range of density ratios. Initial Raman scattering measurements, being proportional to density, provided similar spread rate if twice the FWHM of the radial density profiles is considered. Radial profiles appear to show similarity behavior but not of the classical type observed for turbulent gaseous jets at far field.

#### INTRODUCTION

As combustion and thrust chamber pressures are raised to benefit performance and/or efficiency in cryogenic rocket and turbine engines, the injected liquid fuel may experience an ambient under thermodynamic supercritical condition. As examples, the Space Shuttle main engine thrust chamber pressure with liquid H<sub>2</sub> (P<sub>c</sub>=1.27MPa, T<sub>c</sub>=33.25K)/liquid O<sub>2</sub> (P<sub>c</sub>= 5.043MPa, T<sub>c</sub>=154.58K) is about 22.3 MPa, and the combustion chamber pressure for Vulcain (Ariane 5) can reach up to 10 MPa. The uniqueness of the situation comes from the fact that for pure substances, the distinction between liquid and gas phases disappears at and above the critical pressure and density, thermal conductivity, mass diffusivity, and surface tension show large variations near the critical point. At sufficiently high ambient pressures, the solubility of gases into the liquid phase becomes important and multicomponent phase equilibrium information, or "critical mixing temperature or pressure," should be used (see Bruno and Ely [3]). The terms subcritical and supercritical, and the reduced pressure (P<sub>r</sub>) and temperature (T<sub>r</sub>), are defined here with respect to the critical condition of the pure substance used in the jets, and not the environment.

Past efforts by other researchers on this subject can be found in, for example, Newman and Brzustowski [4] and Mayer et al. [5], [6], and Chen and Sui [7] at high Reynolds numbers, and Woodward and Talley [8] at low Reynolds numbers. In summary, they reported gas-jet like visual appearance under supercritical chamber temperature and pressure with no evidence of droplet even though liquid was injected. At low Reynolds numbers and for an N<sub>2</sub>-into-N<sub>2</sub> cryogenic jet, it was shown that the addition of He gas to the supercritical ambient N<sub>2</sub> fluid forced the jet to look like an injection into a subcritical ambient condition. Raman scattering was used by Anderson et al [9], Decker et al. [10], Oswald and Schik. [11], and Oswald et al. [12] to investigate the structure of the nitrogen fluid jet under supercritical condition. In these experiments, Decker et al [10] observed a smooth transition from the high-density core of an N<sub>2</sub> into N<sub>2</sub> jet toward the gaseous outer region; that is, there was no distinct phase interface. The density radial profile was never a top-hat even as close as a distance-to-diameter ratio of 2.5. Based on limited tests, they concluded that the thermodynamic state of an injected supercritical fluid is of prime importance in the jet growth and not the injection velocity or momentum.

Approved for public release; distribution unlimited.

extra 's' ?

He is Sunday + sig. page says 173

extra

extra space

extra space

an ambient what? pressures?

no ital.

The objective in this paper is to concisely present our experiences learned so far on injection under supercritical condition through experimental and modeling efforts.

## DESCRIPTION OF THE TEST RIG

The stainless steel chamber in Fig. 1 can withstand pressures and temperatures of up to 137 atm (2000 psi) and 473 K, respectively, and has two facing circular sapphire windows and two UV-grade side-mounted slot-shaped quartz windows for laser in/out of the chamber. Transport of the liquid through the lines and the injector is achieved as shown in Figure 1. The liquid N<sub>2</sub> from a dewar is used to cool and/or liquefy the injectant passing through the cryogenic cooler prior to injection. In addition to N<sub>2</sub>, a branch is connected for possibly introducing other gases or mixtures of gases as a chamber medium. The mass flow rate of the injectant is regulated and also measured via a mass flowmeter, and a precision micrometer valve. For more details refer to Woodward and Talley [8] and Chehroudi et al. [13]. The injection in this study is through a sharp-edged 50 mm long stainless steel tube with 1.5 mm (1/16") diameter and a 25 micron (0.010") inner hole (length-to-diameter ratio of 200). With the Reynolds number ranging from 25,000 to 70,000, the entrance length from 50 to 100 is needed (see Schlichting [14]). The length is therefore long enough to ensure fully developed turbulent pipe flow at the exit. The rig is fully instrumented with thermocouples, pressure gages and transducers, and mass flowmeters at the locations indicated in Fig. 1. Back-illumination and a model K2 Infinity long-distance microscope is used with a TM-745E high resolution [768(H) x 493(V) pixels in 8.8(H)x6.6(V) mm actual sensing area] interlaced CCD camera by PULnix to form images of the injected jets. For more details refer to Chehroudi et al. [13].

the jet. Major structural/interface changes occurred at about  $P_r$  of 1.03. No drops were detected, thread- or finger-like entities at the interface were not broken up into droplets but dissolved at different distances from the jet central dense-core region. This created a mixing layer in which phase transition and/or large local density non-uniformities occurred. A further increase in chamber pressure, decreased the length and the thickness of the central dense-core and images progressively appeared similar to an injection of a gaseous turbulent jet into a gaseous environment (see images in Fig. 2). Aligned with what reported before, no evidence of drop formation was seen in this gas-like jet regime. The reason for this

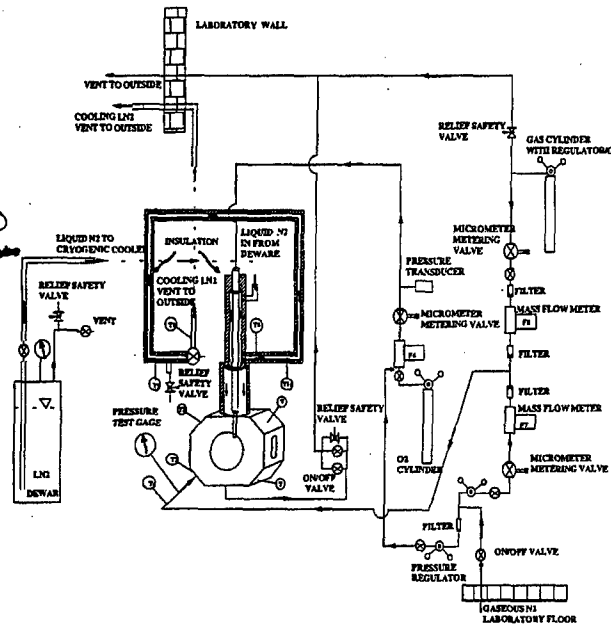


Figure 1. Schematic diagram of experimental setup for sub- to supercritical jet injection

## EXPERIMENTAL AND MODELING EFFORTS

In this section, the authors' experiences learned at the AFRL are described and summarized to this date. First, structural changes observed using shadowgraphy are explained. Second, results of our fractal analysis is presented and briefly discussed. Third, our initial attempt to model the measured growth rate of the jet is presented. Finally, our recent effort using laser diagnostics via Raman scattering to measure density profiles and growth rate is briefed. This will provide a summary of our important findings and achievements regarding injection under supercritical condition.

## VISUAL CHANGES OF THE JET

Using liquid N<sub>2</sub> injection into gaseous N<sub>2</sub> ambient when chamber pressure was far lower than the critical pressure of the jet substance (i.e. subcritical chamber pressure), the jet was observed to be liquid-like with surface instabilities that grew downstream from the injector. Also, very fine drops were detected ejecting from

metamorphic behavior is to be sought in progressive reduction of surface tension and heat of vaporization until they both are sufficiently reduced near and above the critical point. Similar observations were made for the O<sub>2</sub>-into-N<sub>2</sub> case but with the transition to gas-like jet at near the oxygen critical pressure ( $P_r = 0.85$ ). In Fig. 2, as chamber pressure approaches the critical condition, surface tension is reduced to a near-zero value and for the range of Reynolds number used here (25,000 to 75,000), the Ohnesorge number sharply swings from a low (estimated to be  $2.8 \times 10^{-3}$ ) to a very large (infinity when surface tension is zero) values. At the low Ohnesorge number in this work, the so-called second-wind induced liquid jet breakup behavior is observed, see Fig. 2. Past this stage, and before reaching the full atomization, the surface tension is sufficiently and rapidly reduced to produce a gas-like jet appearance near but before reaching the critical pressure value (see Fig. 2). The aforementioned threads or fingers are gasified and no drops are detected. Transition into a full atomization regime is therefore inhibited by this mechanism.

## QUANTITATIVE MEASURE OF THE JET GROWTH RATE

The jet growth rates or spread angles were measured from the images and only to within a  $7\text{-mm}$  distance from the injector exit plane (distance-to-diameter ratio of up to 28). Based on the intact core measurements of the liquid sprays and potential core of the gaseous jets (Chehroudi *et al.* [13]) showed that this measurement distance was well within the mixing layer region and that comparison with classical mixing layers was justified (see Chehroudi *et al.* [19] and Abramovich [18]). Detailed discussion of the choices of the data set in Fig. 3 is given elsewhere in our published work (see Chehroudi *et al.* [13]).

The simplest curves in Fig. 3 are the prediction of the linear jet growth for turbulent incompressible submerged jets using the mixing length concept and a semi-empirical equation by Abramovich [18] incorporating the effects of density variations using a characteristic velocity. The growth rate measurements by Brown and Roshko [20] in a subsonic two-dimensional incompressible turbulent mixing layer between helium and nitrogen are shown in Fig. 3. Also, the independently-derived theoretical equations proposed by Papamoschou and Roshko [2] and Dimotakis [1] for incompressible variable-density mixing layers are shown.

Because of the liquid-like and gas-like appearances of the jet, the growth rate for liquid sprays from single-hole nozzles typical of the ones used in diesel engines are also shown. We selected the steady isothermal spray-angle information by Reitz and Bracco [15] and Hiroyasu and Arai [21] at two different nozzle length-to-diameter ratios with their corresponding vertical error-bands indicating experimental scatter. In addition, a theoretical equation derived by Reitz and Bracco [15] is shown. As a cross check, a recent curve-fitted equation to experimental data from transient sprays proposed by Naber and Siebers [22] is also shown. Their angle measurement zone extends beyond our initial region and this to some extent contributes to disagreement seen between the two sets of data for liquid sprays at injector length-to-diameter density ratio of about 4, see Fig. 3.

Figure 3 covers a density ratio of nearly four orders of magnitude, from liquid sprays to supersonic mixing layers, a unique and new plot on its own right. Disagreements seen between the measured data can to some extent be attributed to differences in the definition of the mixing layer thicknesses and their measurement methods (see Chehroudi *et al.* [13]). The constant spread-angle results of incompressible turbulent jet overpredicts nearly all others in Fig. 3. Disagreement between the turbulent gas jet by Abramovich [18] and incompressible variable-density model of Papamoschou and Roshko [2] increases as density ratio increases. It is clear that for a range of density ratios in which our images show gas-jet like appearance, the experimental data agrees well with the proposed theoretical equation by Dimotakis [1] and closely follows

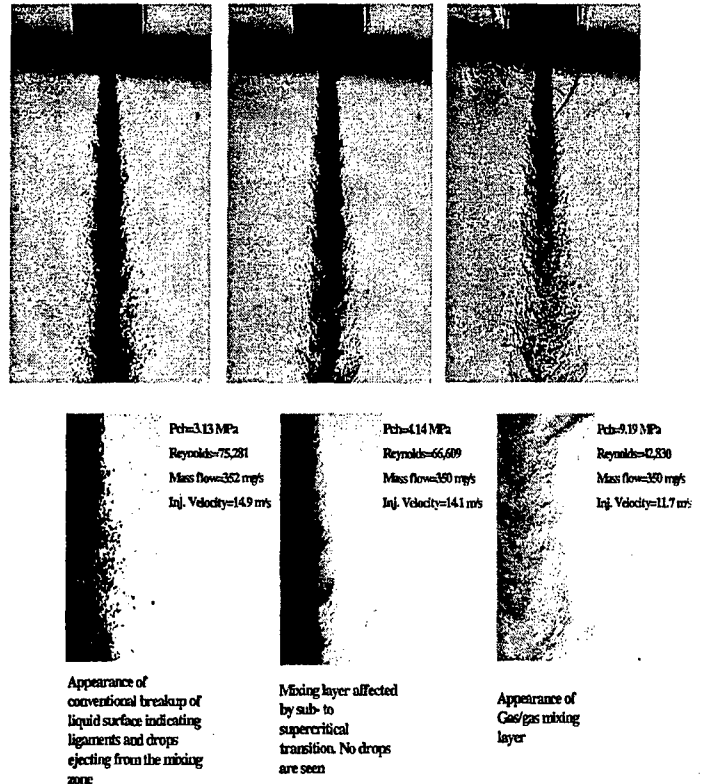


Figure 2. (Top) Back-illuminated images of a cryogenic  $\text{N}_2$  into  $\text{N}_2$  round jet injection at chamber conditions of  $Pr = 0.92, 1.22, \text{ and } 2.7$  but at a fixed supercritical temperature of  $300\text{ K}$  ( $P_{\text{critical}} = 3.39\text{ MPa}$ ;  $T_c = 126.2\text{ K}$ ).  $Re = 25,000$  to  $75,000$ , Fround number:  $40,000$  to  $110,000$  (momentum-dominated jet), injection velocity:  $10\text{-}15\text{ m/s}$ , and injectant temperature:  $99$  to  $110\text{ K}$ . (Bottom) Software-magnified images of the edge of the jet in transition to the gas-jet like appearance is seen starting at just below the critical pressure of the injectant. A gradual transition from a classical liquid-like appearance in which ligaments and drops are formed at the boundary in the liquid atomization regime to a comb-like structure near the critical point, and finally to where a submerged turbulent gas jet appearance emerges can be observed.

the trend of Papamoschou and Roshko [2]. This was the first quantitative confirmation that at an injected jet under supercritical pressure and temperature ambient conditions (based on the pure injectant), grows similar to a gas jet. Even though the jet investigated here appears to go through initial phases of the liquid atomization process, there is a marked disagreement at above the critical condition in both the magnitude and slope between the liquid sprays (at a comparable length-to-diameter ratio of 85) and our data in Fig. 3. It appears that although the jet studied here shows second wind-induced breakup features similar to liquid jets, it fails to reach full atomization state as chamber pressure (really density) is raised. This is because the thermodynamic state approaches the critical point and consequently both surface tension and heat of vaporization are reduced to sufficiently low values.

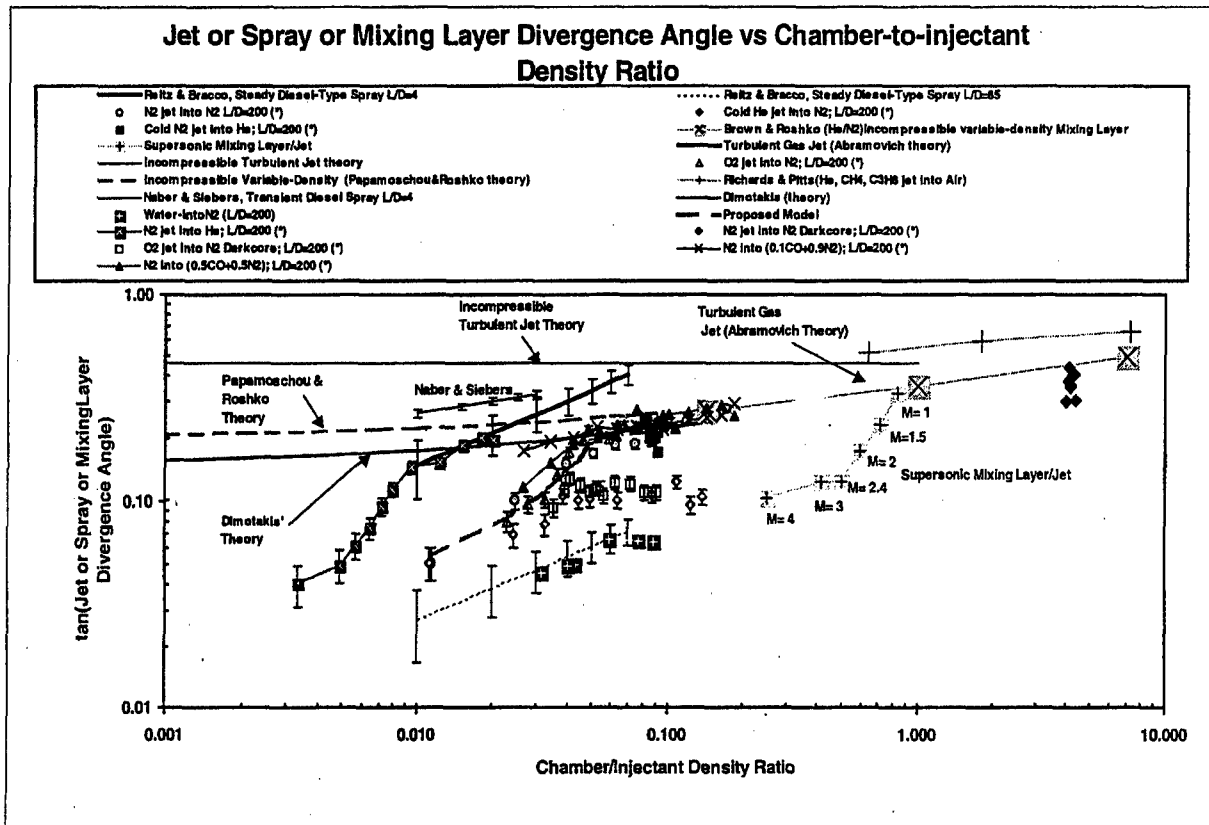


Figure 3. Shows spreading or growth rate as a tangent of the visual spreading angle versus the chamber-to-injectant density ratio. (\*) refers to data taken at AFRL. ~~stet~~

### FRACTAL ANALYSIS OF THE JET

This appeared to be a suitable analysis method to investigate the morphology of the interfacial phenomena and in recent years a number of applications of fractal analysis have been demonstrated in different disciplines. For a concise description and methodology refer to *Chehrودي et al.* [23]. For example, *Sreenivasan and Meneveau* [24] computed the so-called fractal dimension of the turbulent/non-turbulent boundary of an incompressible axisymmetric gaseous jet and reported a value of 1.33 using two-dimensional slicing by a laser sheet. *Sreenivasan* [24] also reported values of 1.35, 1.34, and 1.38 for a round gaseous jet, a plane gaseous mixing layer, and a boundary layer flow, respectively. Figure 4 shows results of plotting the fractal dimension applied to the  $N_2$ -into- $N_2$  jets as a function of relative chamber pressure. In this figure the fractal dimension by other researchers in the gaseous jets, mixing layer, and boundary layers are also shown. The key observation here is that the average value measured for our jet reaches very near those of gaseous jets and mixing layers when ambient pressure goes above the critical point of the injectant. This is considered as an additional quantitative confirmation of the gas-like jet behavior indicated earlier through our growth rate measurements in this same region. As pressure (density) is decreased below  $P_r$  of about 0.6, the fractal dimension is rapidly reduced towards the Euclidean

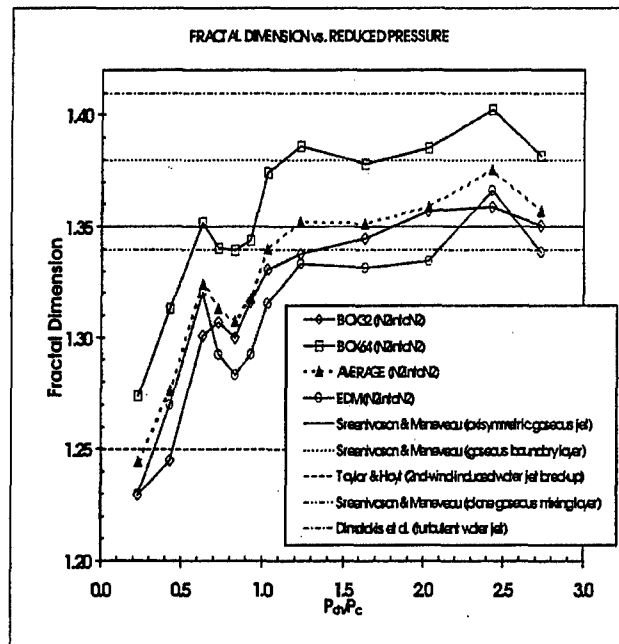


Figure 4. Box-counting and Minkowski (Euclidean Distance Mapping (EDM) algorithm) fractal dimensions of the visual boundary of the jet as a function of the reduced chamber pressure for  $N_2$ -into- $N_2$  injection.

value of 1 for a smooth circular cylinder with no surface irregularities. Considering the geometric interpretation of the fractal dimension, measured values are quite consistent with the visual observations of jet interface changes in our tests. For more details, see *Chehroudi et al.* [23].

### MODELING OF THE GROWTH RATE

As no analytical treatment exists starting from basic principles, the idea was to intelligently search for a form of an equation based on an intuitive and physically reasonable model that can predict the jet growth rate data presented in Fig. 5. In essence, the proposed approach is to employ two appropriate characteristic times of the problem, combined with a hypothesis and the growth rate equations for isothermal liquid sprays and gaseous mixing layers to propose an "intuitive/smart" equation that is capable to closely represent the growth rate information measured for the sub- and supercritical conditions presented before.

Consider injection into a subcritical pressure environment similar to the ones shown in Fig. 2. Here, an appropriate characteristic time is the "bulge" formation/separation time ( $\tau_b$ ) pertaining to the interface of turbulent liquid jet where isolated ligaments and drops are produced through primary atomization. *Tseng et al.* [26] suggested that  $\tau_b = (\rho_l L^3 / \sigma)^{1/2}$  for the primary breakup of turbulent liquid jets. Here,  $\rho_l$ ,  $L$ , and  $\sigma$  are liquid density, characteristic dimension of turbulent eddy, and surface tension, respectively. The second characteristic time (at subcritical pressures) is the gasification time ( $\tau_g$ ) calculated through the so-called D-square law for drops and is equal to  $D^2/K$  where  $D$  and  $K$  are drop diameter and vaporization constant, respectively. In addition, we also propose a hypothesis that if the aforementioned characteristic times (calculated for appropriate length scales) are nearly equal in magnitude, then the interface bulges are not able to separate as unattached entities from the jet interface to form ligaments

and drops because they are gasified as fast as they desire to be detached. In a sense, this is defined as the onset of the gas-jet like behavior.

It was indicated earlier that the jets investigated here showed both liquid-like and gas-like behaviors and that the growth rate of the latter agrees well with those of incompressible variable-density gaseous mixing layers. Therefore, forms of the growth rate equations for the liquid sprays as well as incompressible variable-density gaseous jets are considered. For liquid sprays, using linear instability theoretical analysis, *Reitz and Bracco* [15] proposed the following equation for the isothermal liquid spray growth rate:  $\theta_s \approx 0.27 [0 + (\rho_g/\rho_l)^{0.5}]$ , where  $\theta$  is spray full-cone angle. Also, from *Brown/Papamoschou/Rashko's* theory for an incompressible variable-density gaseous mixing layer one can derive an equation,  $\theta_{BPR} \approx 0.212 [1 + (\rho_g/\rho_l)^{0.5}]$ , where  $\theta$  is the visual jet full-cone angle. Finally, based on a different theoretical treatment by *Dimotakis* for incompressible variable-density gaseous mixing layers, an

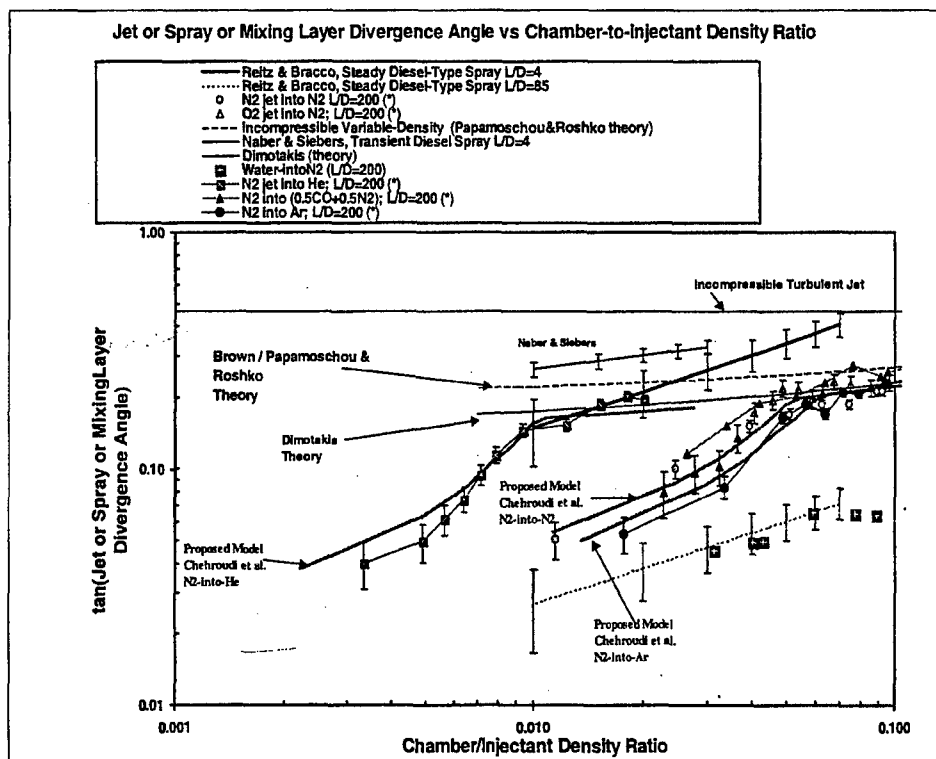


Figure 5. Comparison of the proposed growth rate model with the experimental data for the sub- to supercritical jet. (\*) refers to data taken at AFRL.

equation of the form  $\theta_D \approx 0.265 [0.59 + (\rho_g/\rho_l)^{0.5}]$  can be derived. The similarity of these equations is remarkable despite their different theoretical treatments. The following "intuitive/smart" form of an equation describing the growth rate for both sub- and supercritical jets is therefore proposed:  $\theta_{Ch} \approx 0.27 [(\tau_p/(\tau_b + \tau_g)) + (\rho_g/\rho_l)^{0.5}]$  (see *Chehroudi et al.* [23] for more details). In a sense, a physical meaning is attributed to the first term in the

bracket and it is linked to the physical picture hypothesized earlier. Note that, in the limit, this equation collapses to the isothermal liquid spray case when  $\tau_g \gg \tau_b$  and  $\tau_g \rightarrow \infty$ .

must reference figure before the figure is shown

Figure 5 shows comparison of the proposed model equation with the characteristic time ratio calculated for the  $N_2$ -into- $N_2$  case. Good agreement is observed. For cases other than the  $N_2$ -into- $N_2$ , such as  $N_2$ -into-He or  $N_2$ -into-Ar, due to lack of reliable information on thermodynamic properties and in particular the surface tension. To model these cases, it was proposed that the characteristic time ratio  $\tau_b/(\tau_b + \tau_g)$  is a dominant function of the density ratio only, i.e.  $\tau_b/(\tau_b + \tau_g) = F(\rho_g/\rho_l)$ . As Brown and Roshko [20] indicated, this is a reasonable behavior to consider because at low Mach number squared values there is no distinction between mixing layers made of two streams with differences in molecular weights, differences in temperature, and high speed compressibility effects (see also Chehroudi et al. [13]). It was shown that the same function  $F(\rho_g/\rho_l)$  calculated through measurements for the  $N_2$ -into- $N_2$  case could be made to work for other cases provided a case-dependant transformation is made to the density ratio at which F is evaluated. The quality of the agreement with experimental data is demonstrated in Fig. 5 and considered to be good.

### RAMAN SCATTERING MEASUREMENTS

When a transparent medium is irradiated, some fraction of the beam is scattered in all directions. Raman, in 1928, discovered that the wavelength of a very small fraction of the scattered radiation by certain molecules shifted in an amount dependent upon the chemical structure of the molecules responsible for the scattering. It can be shown that the intensity of the signal is proportional to the density of the observed molecule. In our case, an Nd:YAG pulsed laser beam at 532 nm was used with a passive pulse stretcher to change the pulse duration from 10 ns to about 36 ns. This was done to minimize the occurrence of the stimulated Raman effects particularly at sub- and near-critical condition (see Anderson et al. [9]). The transmitting optics created a controllable sheet of laser with precise traversing capabilities in two directions. The scattered light at 607 nm is detected by a 256x256 CCD camera equipped with suitably-chosen number of filters to maximize the signal-to-noise ratio. For more details on experimental setup and data acquisition refer to Chehroudi et al. [27].

The integrity of the entire Raman measurement system was tested by measurement of the density of a pure nitrogen gas in the high-pressure chamber for several pressures. Measured to calculated (based on ideal gas law) density ratios agreed to within 2%. Figure 6 shows intensity defect, being proportional to the density defect, radial plots at sub- and supercritical conditions. It is clear that as chamber pressure is increased the intensity level

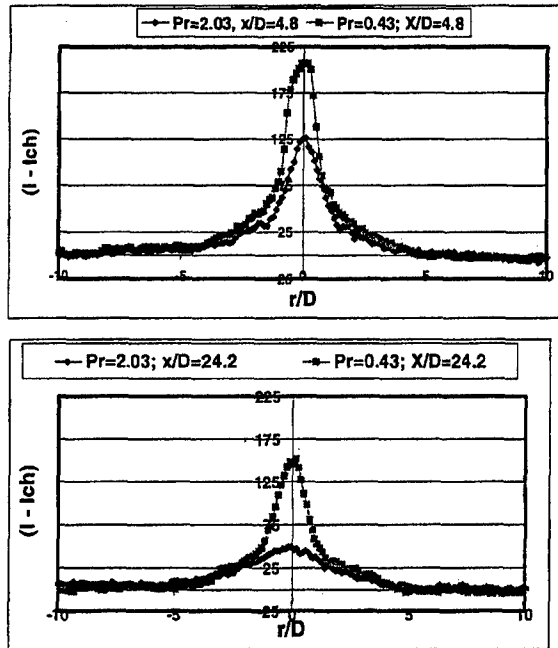


Figure 6. Radial plots of  $(I - I_{ch})$ , the Raman intensity  $(I)$  from the jet as measured with reference to that of the chamber gas  $(I_{ch})$  for the  $N_2$  into  $N_2$  case under sub- and supercritical conditions and at two different axial positions.

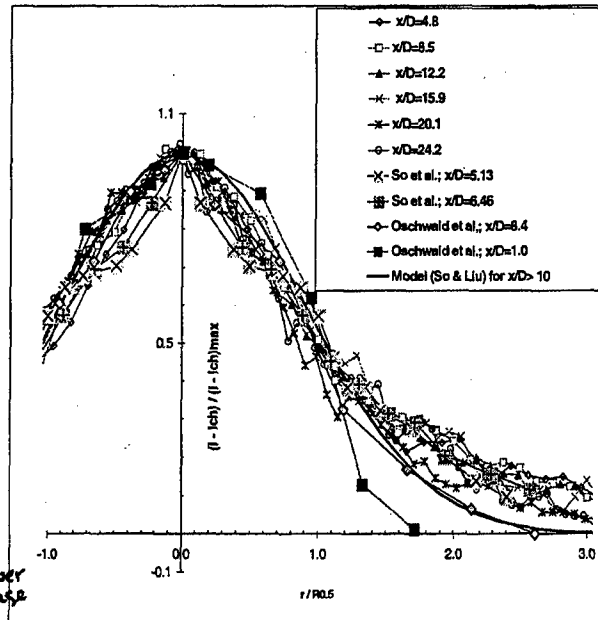
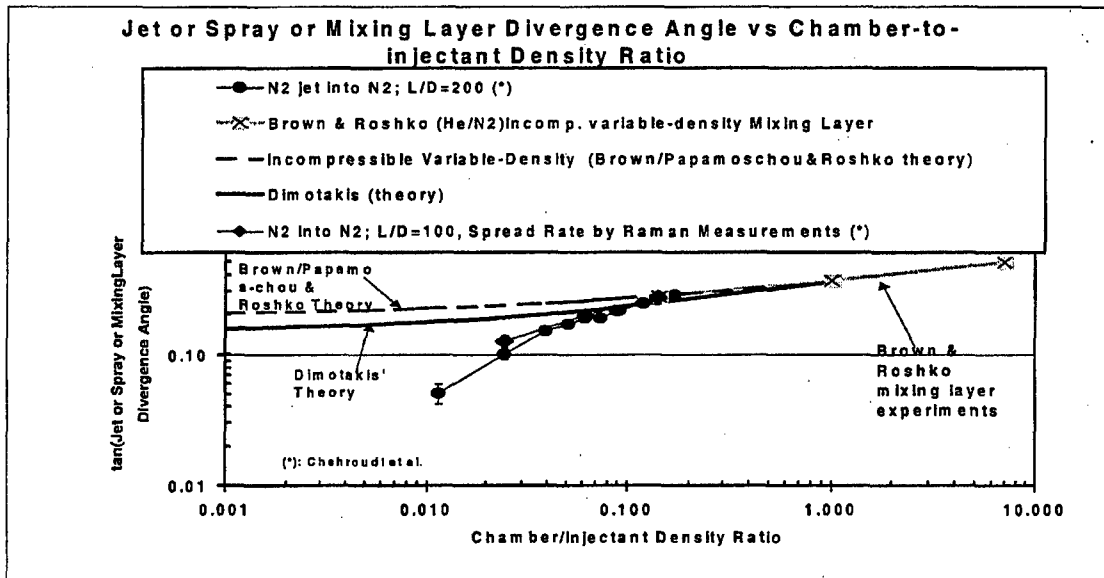


Figure 7. Normalized plots to inspect similarity behavior in comparison to gaseous jet results. Laser enters from right to left.  $N_2$  into  $N_2$  at supercritical chamber condition.

drops down in the central region due to larger spreading of the jet. The data for the subcritical case should be considered with reservation particularly at larger radial positions due to reflection of the laser from the jet's well-

reference Fig 7 before its shown



reference  
Fig 8  
reference is  
shown

Figure 8. Plot of the spread rate as measured by Raman intensity radial plots at twice the FWHM shows good agreement with our earlier measurements using shadowgraphy technique.

defined boundary causing broadening of the profiles. This issue is addressed in more details in *Chehroudi et al [27]*. If the jet exhibits gas-like behavior one might attempt to compare the results with those of gaseous jets to see extent to which they simulate each other. A normalized plot format is used for this purpose in Figure 7. Here, results at supercritical condition and for different axial positions are shown along with a similarity-type model equation generally accepted for turbulent jets, and at larger axial distances than those shown in this figure. Even though some degree of similarity is exhibited, they are not of the type observed in the far field region for turbulent gaseous jets. Actual density measurements in gaseous jets made by *So et al. [28]* in comparable nondimensionalized axial distances indicate reasonable agreement within the experimental accuracy (see Fig. 7). Results by *Oschwald et al. [12]* are also shown but no conclusion is drawn at this time due to differences in initial conditions between the two sets of data known to affect jets and sprays spreading. The full width of the radial profiles measured at the half maximum (FWHM) is extracted from the Raman measured data. They are believed to be unaffected by the broadening observed at the edge of these profile. When spread rate is calculated based on twice the FWHM values of Raman radial profiles and plotted along with other measurements in Fig. 8, it shows good agreement with our earlier results using shadowgraphy method. This can be considered as a correspondence calibration of the two different techniques of estimating the width of the jet investigated here.

#### SUMMARY AND CONCLUSIONS

Metamorphic behavior and growth rates of jets injected into an environment at a given supercritical

temperature but varying pressure are analyzed. At subcritical chamber pressures, the injected fluid appears to undergo the classical liquid jet breakup stages up to a second wind-induced breakup regime with discernable ligaments and droplets. Penetration into the full atomization regime is inhibited near the critical pressure of the injectant because of the combined effects of lowered surface tension and heat of vaporization. At this point the visual structure of the changes to a gas-jet like appearance and remains up to the highest pressure tested. Also, a unique and comprehensive plot on growth rate is formed using the most relevant works of other researchers covering an ambient-to-injectant density ratio range of four orders of magnitude. Our measured jet growth rates via shadowgraphy follow the theoretical equations proposed by *Papamoschou and Roshko [2]* and *Dimotakis [1]*, both derived for incompressible variable-density gaseous turbulent mixing layer. This agreement starts at a pressure near but below the thermodynamic critical pressure of the injectant, quantitatively supporting the observed gas-jet like visual appearance of the supercritical jets for the first time. The geometry of the jet interface has also been examined for the first time by fractal analysis. The results clearly indicate a transition from a Euclidean to a fractal interface, with a fractal dimension close to values measured for gaseous turbulent jets. This provides additional quantitative evidence for the hypothesis that the jet evolves into a gas-like behavior. An "intuitive/smart" equation is proposed that agrees well with the experimental growth rate data, based on a proposed physical mechanism and characteristic gasification times and interfacial bulge formation/separation times. Initial Raman scattering measurements from the jets confirms the

front  
jet  
lane

growth rate measured via shadowgraphy provided. Twice the FWHM of the  $\rho$  density radial profiles are used. The density defect plots show tendency to be similar but not of the type observed for turbulent gaseous jets at far field.

## ACKNOWLEDGEMENTS

The authors would like to thank Mr. Mike Griggs for machine-shop work and assisting in setup modifications. Mr. Earl Thomas is thanked for his valuable support in this project. We appreciate Mr. Theodore Miles's effort in searching copies of many requested publications. In particular, Mr. Paul Loftsgard is thanked for his assistance in part of the data acquisition/processing and most of the fractal analysis work. Professor A. Badakhshan, summer faculty visitor, is thanked for his contributions on initial setup and testing of the Raman measurement system. This work is sponsored by the Air Force Office of Scientific Research under Mr. Mitant Birkan, program manager.

## REFERENCES

1. Dimotakis, P. E. "Two-dimensional shear-layer entrainment," AIAA Journal, 21, No. 11, 1986, pp. 1791-1796.
2. Papamoschou, D. and Roshko, A. "The compressible turbulent shear layer: an experimental study," J. Fluid Mech., vol. 197, 1988, pp. 453-477.
3. Bruno, T. J. and Ely, J. F. Supercritical fluid technology, CRC Press, 1991.
4. Newman, J. A. and Brzustowski. "Behavior of a liquid jet near the thermodynamic critical region," AIAA Journal, vol. 9, 1971, no. 8, pp. 1595-1602.
5. Mayer, et al. "Injection and mixing processes in high pressure LOX/GH2 rocket combustors," AIAA Paper no. 96-2620, Lake Buena Vista, Florida, 1996.
6. Mayer, et al. "Propellant atomization in LOX/GH2 rocket combustors," AIAA Paper no. 98-3685, 1998.
7. Chen, L.-D. and Sui, P.-C. "Atomization during the injection of supercritical fluid into high pressure environment," in Mechanics and Combustion of Droplets in Sprays by Chiu and Chigier.
8. Woodward, R. D. and Talley, D. G. "Raman imaging of transcritical cryogenic propellants," AIAA Paper 96-0468, Reno, Nevada, January 1996.
9. Anderson, T. J., Woodward, R. D., and Winter, M. "Oxygen Concentration Measurements in a High Pressure Environment Using Raman Imaging," AIAA Paper 95-0140.
10. Decker, M. C., Schik, A., Meier, U. E., Stricker, R. W. "Quantitative Raman Imaging Investigations of Mixing Phenomena in High Pressure Cryogenic Jets," Appl Opt 37:5620-5627, 1998.
11. Oswald, M. and Schik, A. "Supercritical Nitrogen Free Jet Investigated by Spontaneous Raman Scattering," Experiments in Fluids, 27, 497-506, 1999.
12. Oswald, M., Schik, A., Klar, M., Mayer, W. "Investigation of Coaxial LN2/GH2-Injection at Supercritical Pressure by Spontaneous Raman Scattering," 35th AIAA/ASME/SAE/ASEE Joint Propulsion Conference and Exhibit, Los Angeles, CA, 20-24 June, 1999.
13. Chehroudi, et al. "Initial Growth Rate and Visual Characteristics of a Round Jet into a Sub- to Supercritical Environment of Relevance to Rocket, Gas Turbine, and Diesel Engines," AIAA paper 99-0206, Reno, Nevada, 1999.
14. Schlichting, H. Boundary Layer Theory, MacGraw-Hill Book Company, seventh edition, 1979.
15. Reitz, R. D. and Bracco, F. V. "On the dependence of spray angle and other spray parameters on nozzle design and operating condition," SAE international Congress and Exposition, SAE Paper no. 790494, Detroit, Michigan, February 26-March 2, 1979.
16. Faeth, G. M., "Structure and atomization properties of dense turbulent sprays," Twenty-third Symposium (International) on Combustion, The Combustion Institute, P.1345, 1990.
17. Tseng, et al. "Continuous- and dispersed-phase structure of pressure-atomized sprays," Progress in Astronautics and Aeronautics: Recent Advances in Spray Combustion, February, 1995.
18. Abramovich, G. N. The theory of turbulent jets, M.I.T. Press, 1963.
19. Chehroudi, et al. "On the Intact Core of Full-Cone Sprays," SAE Transaction Paper 850126, 1985.
20. Brown, G. and Roshko, A. "On density effects and large structure in turbulent mixing layers," J. Fluid Mech., vol. 64, 1974, part 4, pp. 775-816.
21. Hiroyasu, H. and Arai, M. "Fuel spray penetration and spray angle in diesel engines," Trans. JSAE, Vol. 21, 1980.
22. Naber, J. D. and Siebers, D. L. "Effects of gas density and vaporization on penetration and dispersion of diesel sprays," SAE Paper no. 960034, 1996.
23. Chehroudi, B., Talley, D., and Coy, E. "Fractal geometry and growth rate of cryogenic jets near critical point," AIAA Paper 99-2489, 35th AIAA/ASME/SAE/ASEE joint propulsion Conference, Los Angeles, CA, June 20-24, 1999.
24. Sreenivasan, K. R. and Meneveau, C. "The fractal facets of turbulence," J. Fluid Mech. Vol. 173, pp. 357-386, 1986.
25. Sreenivasan, K. R. "Fractals and multifractals in fluid turbulence," Annu. Rev. Fluid Mech, Vol. 23 pp. 539-600, 1991.
26. Tseng, L.-K., Ruff, G. A., P.-K., Wu, Faeth, G. M., "Continuous- and dispersed-phase structure of pressure-atomized sprays," Progress in Astronautics and Aeronautics: Recent Advances in Spray Combustion, February, 1995. # 17
27. Chehroudi, B., Badakhshan, A., Talley, D., and Cohn, R. "Raman Scattering Measurements in the Initial Region of Sub- and Supercritical Jets," AIAA Paper 2000-3392, 36th AIAA/ASME/SAE/ASEE Joint Propulsion Conference and Exhibit "Propulsion-Key to Exploring New Worlds" Von Braun Civic Center Huntsville, Alabama 16-19 July 2000.
28. So, R. M. C., Zhu, J. Y., Otugen, M. V., and Hwang, B. C. "Some Measurements in a Binary Gas Jet," Experiments in Fluids, 9, 273-284, 1990.

Don't  
cost  
smaller

Don't  
is different  
size